Powder Technology 303 (2016) 228–240

Contents lists available at ScienceDirect

Powder Technology

journal homepage: www.elsevier.com/locate/powtec

Simulating the DISAMATIC process using the discrete element method — a dynamical study of granular flow

E. Hovad [a,c,*], J. Spangenberg [a], P. Larsen [c], J.H. Walther [a,d], J. Thorborg [a,b], J.H. Hattel [a]

[a] Department of Mechanical Engineering, Technical University of Denmark (DTU), Denmark
[b] MAGMA Giessereitechnologie GmbH, Kackertstr. 11, 52072 Aachen, Germany
[c] DISA Industries A/S, Højager 8, Høje Taastr., 2630 Taastrup, Denmark
[d] Computational Science and Engineering Laboratory, ETH Zurich, CH 8092, Switzerland

ARTICLE INFO

Article history:
Received 4 May 2016
Received in revised form 26 August 2016
Accepted 15 September 2016
Available online 17 September 2016

Keywords:
Sand casting
Green sand
Granular flow
Discrete element method
DISAMATIC process

ABSTRACT

The discrete element method (DEM) is applied to simulate the dynamics of the flow of green sand while filling a mould using the DISAMATIC process. The focus is to identify relevant physical experiments that can be used to characterize the material properties of green sand in the numerical model. The DEM parameters describing the static friction coefficients are obtained using a ring shear tester and the rolling resistance and cohesion value is subsequently calibrated with a sand pile experiment. The calibrated DEM model is used to model the sand shot in the DISAMATIC process for three different sand particle flow rates as captured on the corresponding video footage of the interior of the chamber. A mould chamber with three ribs mounted on the fixed pattern plate forming four cavities is chosen as a reference geometry to investigate the conditions found in the real moulding process. The geometry of the cast part and the casting system can make the moulding process complicated due to obstacles such as ribs that deflect the sand flow causing "shadows effects" around the cavities of the mould. These dynamic effects are investigated by the qualitative flow dynamics and quantitative mould filling times captured in the video footage and simulated by the calibrated DEM model. Both two- and three-dimensional DEM models are considered and found to produce results in good agreements with the video footage of the DISAMATIC process.

1. Introduction

The DISAMATIC process produces moulds made of green sand for metal casting. These sand moulds are typically used for casting metal parts, such as brake disks, crank shafts and engine blocks used in the automotive industry. The DISAMATIC moulding process is illustrated in Fig. 1, showing how the chamber is filled with green sand. The compressed air creates an overpressure in the top of the hopper that drives the flow of the sand through the sand slot down into the chamber. The sand shot is followed by a squeezing step, where the sand is compacted to increase density and build up strength in the sand mould before the casting process.

The green sand consists of quartz sand as the primary component mixed with bentonite and water, which coats the sand grains to form a cohesive granular material. After filling the chamber, the green sand is squeezed (Fig. 1 right) and the material forms bonds to create a stable and relatively strong mould. The quality of the mould is affected by many factors, including the mixture of quartz sand, the complexity of the mould chamber geometry and the compressed air pressure driving the flow of the green sand where the final mould must be homogeneous and stable.

The discrete element method (DEM) is a particle based method that is often used to model granular flow and it has received increased attention in the last decade. The general industrial application areas of the DEM method is typically flow in hoppers, mixers, drums and mills this is all discussed in the review [1]. A general review of the theoretical foundation has been published in [2] and a comparison of different frequently used DEM models is presented in [3]. DEM is gaining popularity as the computational power available to researchers increases and with the introduction of parallel computing in DEM [4] [5]. Newer codes based on the GPU framework are developed as e.g. [6] for realistic simulation of sand behaviour. The GPU framework of [7] was used for simulations of mill charge in [8] applying the GPU for faster simulating millions of a non-spherical particles.

DEM has been used to simulate the sand mould manufacture for the lost foam process [9], where it was suggested that the particle-particle static friction coefficient and rolling resistance are the most important parameters for the flow behaviour. The DEM model in [9] was calibrated with the repose angle of a sand pile. The calibration of the DEM simulation for blade-granular interaction in earth moving equipment was

* Corresponding author at: Produktionstorvet, Building 425, DK-2800 Kgs., Lyngby, Denmark.
E-mail address: emilh@mek.dtu.dk (E. Hovad).

http://dx.doi.org/10.1016/j.powtec.2016.09.039
0032-5910/

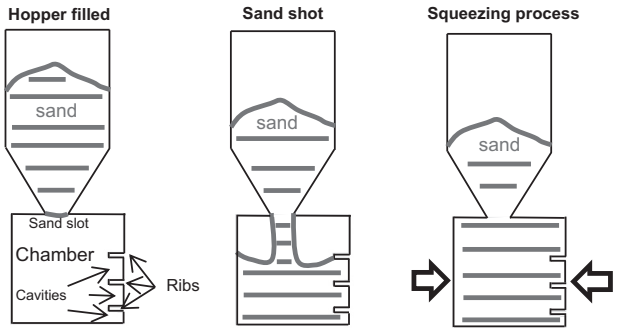

Fig. 1. The sand shot, (left) starts when the hopper is filled with green sand, compressed air from an air receiver (not shown) blows air into the top of the hopper which drives the sand from the hopper through the sand slot into the moulding chamber. In the chamber the cavities and ribs are positioned on the pattern plate positioned on the right hand side (the air exits the chamber through small air vents). (middle) The sand is filling the chamber and its three cavities. (right) Finally when the mould is filled, then the mould is squeezed until the pressure has reached a preset value and the mould is pressed out of the chamber ready for casting and to receive the molten metal. Then the sequence of (left) to (right) can be repeated to construct more moulds.

performed using a direct shear test for calibrating the internal friction angle and a compression test for the estimation of the particle stiffness [10].

DEM simulations of the green sand moulding process have earlier been conducted by [11] with the particle diameter of 6.0 mm and the squeezing process was simulated in [12]. Earlier two-dimensional DEM simulations of the sand shot in the DISAMATIC process [13] were conducted in the simplified chamber geometry illustrated in Fig. 1 focusing on the ribs that deflect the sand flow causing "shadows effects" around the cavities of the mould. The study considered a constant particle inlet velocity and particle diameters of 2 mm and 4 mm as representative sand particles for the granular flow. The sensitivity of the granular flow was studied with respect to the particle-particle rolling resistance and particle-particle static friction coefficient in [13]. The study found that the particle inlet velocity was of greater importance for the results than the particle parameters tested.

In the present study of the DISAMATIC process the sand slot particle inlet velocity and particle flow rate is estimated by using the filling times of the different parts of the mould chamber from video footage. In addition the DEM model is calibrated from experiment to obtain the rolling resistance, cohesion, static friction coefficients assuming a 2 mm particle diameter. Finally a comparison is performed between a two- and three-dimensional DEM model simulating the DISAMATIC process for three different compressed air pressures.

The 2-D simulation appears to give an overestimated energy transfer compared to the 3-D simulations due to the larger number of particle-particle interactions and the additional degrees of freedom in 3-D. The particles in 3-D display a stronger scatter at later filling times as compared to the 2-D simulations.

2. Method: Testing green sand

In the DISAMATIC process compactability testing of the sand is performed done to guarantee the quality of the mould for the subsequent casting step. However, this does not provide sufficient information about the flowability of the sand mixture and it is of great interest to develop new test methods and procedures to characterize the sand flow. This is of particular importance for geometrically complex castings where it can be a challenge to ensure a homogeneous filling, which in turn is needed for the subsequent compaction step.

2.1. Purpose of the experiments: Finding the DEM parameters

The DEM particle density for the 2-D simulations ($\rho_{DEM,2D}$) and 3-D simulations ($\rho_{DEM,3D}$), is found from a ramming test, see Fig. 2.

Fig. 2. Green sand (left), sieving the green sand into the cylinder (middle) and the ramming station used to determine the compactability of the sand mixture (right).

The static friction coefficient for the green sand-green sand interaction and the static friction coefficient for the green sand-steel plate interaction were found from the ring shear tester of the type RST-SX. The values found from the ring shear tester are used for the DEM model to obtain the particle-particle static friction coefficient ($\mu_{s,\,p\text{-}p}$) and the particle-wall friction coefficient ($\mu_{s,\,p\text{-}w}$).

With a sand pile experiment, the parameters investigated in the DEM calibration are the rolling resistance modelling the non-uniform sand particles resistance to rolling and the cohesion value modelling the binding of the green sand due to the bentonite. The cohesion value, $W_{p\text{-}p}$ and the rolling resistance, $\mu_{r,\,p\text{-}p}$ are found from the sand pile experiment by matching the corresponding height of the sand pile, h_p. Calibration simulations are performed to study the effect of these parameters on the height of the final sand pile.

2.2. The green sand

The green sand consists of quartz sand as primary component mixed with bentonite which together with water coats the quartz sand and makes the sand mixture cohesive and sufficiently strong when the mould is finally squeezed.

2.3. Standard testing of green sand

The standard procedures for testing the green sand is from the American Foundry Society (AFS) and described in [14] where the following two standard tests were conducted in the present study: the water content and standard ramming test. For the standard ramming a standard specimen tube was used where the initial green sand sample was weighted before compaction and since the volume was known the density of the un-compacted and compacted green sand test sample could be calculated. The ramming test was conducted with the standard of 3 strokes and to find the maximum density 10 strokes were executed. The green sand values from the standard tests can be seen in Table 1.

2.4. Ring shear tester

The ring shear tester of the type RST-SX is described in [15].

Table 1
Material values for the green sand used for the sand pile experiment.

Material properties	Avr.	Std.	Measurements
Green sand water content	3.6%	0.2%	11
Average compactability level (AFS standard)	42%	0.7%	7
Average maximum compactability (10 ramming)	47%	0.9%	7
Average loose density	832 kg/m^3	11 kg/m^3	14
Average maximum density, ρ_{bulk} (10 ramming)	1557 kg/m^3	8.8 kg/m^3	7

2.4.1. Internal friction angles (φ)

The ring shear tester is used to find flow properties as the three internal friction angles:

- The linearized yield locus, φ_{lin}
- The effective angle of friction, φ_e
- The angle of internal friction at steady-state flow, φ_{sf}

These three internal friction angles and the cohesion of the material (τ_c) can be seen in Fig. 3.

The linearized yield locus, μ_{lin} is the tangent to both the Mohr stress circles defining σ_c and σ_1.

From the ratio of the shear stress, τ_{pre} to normal stress, σ_{pre} a friction angle can be found from the angle of internal friction at steady-state flow, φ_{sf} from the pre-shear point, $\varphi_{sf} = tan^{-1}(\tau_{pre}/\sigma_{pre})$ and the effective internal friction angle, φ_e is defined as the ratio of the minor principal stress, σ_2 to the major principal stress, σ_1 at steady-state flow, $\sin(\varphi_e) = (\sigma_1 - \sigma_2)/(\sigma_1 + \sigma_2)$.

For poorly flowing bulk solids e.g. moist clay the effective angle of internal friction, φ_e can become large compared to the angle of internal friction at steady-state flow, φ_{sf} for the bulk solids layers that are sliding against each other as they do in a shear test during steady-state flow [15]. Thereby the angle of internal friction at steady-state flow, φ_{sf} and the linearized yield locus, φ_{lin} are used as indicators for the DEM models particle-particle internal friction interval. The cohesion of the material, τ_c is defined at zero normal stress ($\sigma = 0$).

Note that the DEM model particle-particle cohesion value, $W_{p\text{-}p}$ together with the rolling resistance, $\mu_{r,\,p\text{-}p}$ is found from the sand pile experiment by the corresponding height of the sand pile, h_p.

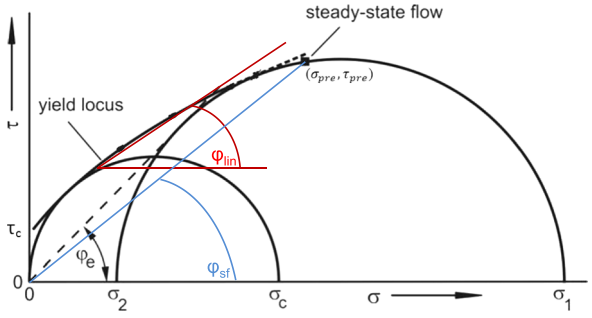

Fig. 3. Yield locus and the three internal friction angles: φ_e (black dotted line) is the linearized yield locus, φ_{lin} (green line) is the effective angle of friction and φ_{sf} (blue line) the angle of internal friction at steady-state flow from the pre-shear point (σ_{pre},τ_{pre}). The normal stress is in the x-axis (σ) and the shear stress is in the y-axis (τ). The major principal stress is $\sigma_1$and the minor principal stress $\sigma_2$for the confined sample (large circle) and the major principal stress is σ_c for the unconfined sample (small circle). The cohesion value found from the ring shear tester of the material is denoted τ_c. Note the edited figure is originally from [16] and the theory is from [15]. (For interpretation of the references to color in this figure legend, the reader is referred to the web version of this article.)

2.4.2. Wall friction angle (φ_x)

To find the wall friction angle, also called the wall yield locus, a bulk sample is subjected to a selected normal load (σ_{w1},σ_{w2}, σ_{w3},…). When a constant shear stress is reached the points (σ_w, τ_w) are recorded as shown in Fig. 4.

The sliding friction angle is found from the slope of the wall yield locus.

2.5. The sand pile experiment

The sand pile experiment is used for estimating the rolling resistance and cohesion in the DEM model and the experimental setup is shown in Fig. 5.

First the hopper is filled with green sand through the sieve having a hole size of 3.5 mm–4.0 mm shown in Fig. 5 (left). After that the orifice is opened rapidly emulating an instantaneous opening of the orifice in the hopper simulation. The height of the sand pile (h_p) from the experiment is illustrated in Fig. 5 (right), and it is defined by the maximum height of the sand pile. This height is measured with a laser projected onto a ruler. In order to allow a 2-D model approach either through a 2-D DEM model or a 3-D slice, the hopper was designed with a long side (l) compared to the width (w_2) of the box with the ratio of $l/w_2 = 0.4$.

3. Numerical method

3.1. Discrete element method (DEM)

The commercially available software STAR-CCM+ is used for the simulations to allow studies of flow in the complex geometry [17]. In DEM the forces are decomposed into a normal and tangential direction, as originally proposed by [18]. The Hertz-Mindlin contact model is chosen due to its ability to obtain the normal and tangential stiffness from real material parameters. Hertzian contact mechanics is used in the normal direction of impact [19] and a simplified Mindlin model is used in the tangential direction of impact [20], from which the non-linear damping can be derived. The non-linear damping model was tested in Refs. [21,22]. The selected model for rolling resistance is the constant torque method first developed by [23] and tested in [24]. The cohesion model selected is the Johnson-Kendall-Roberts (JKR) model described in [25].

3.2. Particle kinematics

The notation applied for describing the equations applied in DEM is from [26], where the two particles in contact is denoted $\{i,j\}$ positioned at $\{\boldsymbol{r}_i, \boldsymbol{r}_j\}$ with the velocities $\{\boldsymbol{v}_i, \boldsymbol{v}_j\}$ and angular velocities $\{\boldsymbol{\omega}_i, \boldsymbol{\omega}_j\}$. The distance between the two particles is denoted

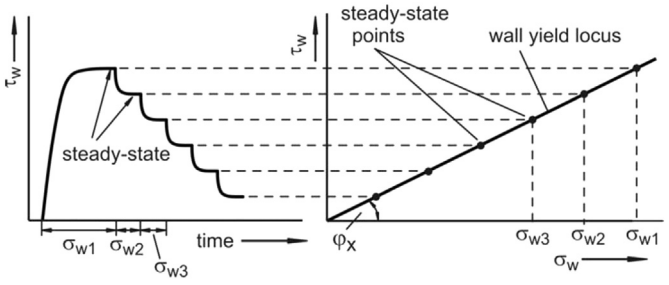

Fig. 4. The selected normal loads (σ_{w1},σ_{w2}, σ_{w3},…) and the shear stresses history, τ_w (left figure). Wall yield locus found from the steady-state points (right figure). Note the edited figures is from [16].

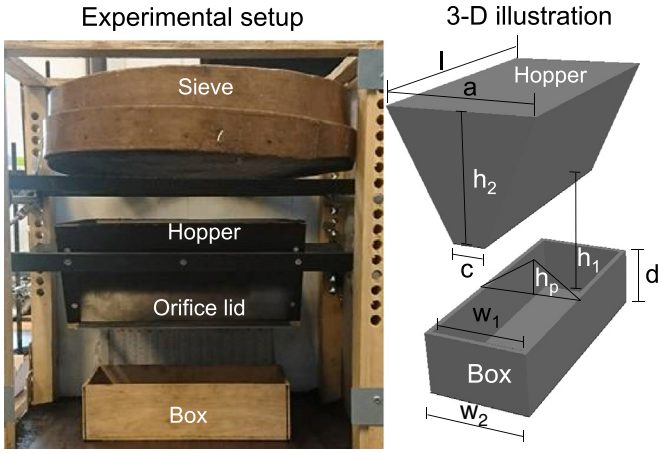

Fig. 5. (Left) The hopper experiment can be seen with the Sieve on the top, the hopper, orifice lid and finally the box in the bottom. (Right) In the 3-D illustration the hopper measurement can be seen with the length l = 300 mm, width of a = 180 mm, orifice c = 40 mm and the box measurements with the internal width $w_1 = 120$ mm, external width $w_2 = 134$, the height of the box d = 82 mm, the measured height of the sand pile is denoted h_p, and the drop height of $h_1 = 169$ mm and hopper height of $h_2 = 150$ mm. Note the box side and bottom thickness is 7 mm.

$r_{ij} = \|\boldsymbol{r}_i - \boldsymbol{r}_j\|_2$, the position vector from particle j to i is $\boldsymbol{r}_{ij} = \boldsymbol{r}_i - \boldsymbol{r}_j$, and the normal overlap $\delta_{n_{ij}}$ is

$$\delta_{n_{ij}} = (R_i + R_j) - r_{ij} = 2R - r_{ij} \tag{1}$$

Since all the particles have the same radius and physical properties $(R_i + R_j) = 2R$ for the particle-particle interaction. The relative normal velocity is

$$\boldsymbol{v}_{n_{ij}} = \left(\boldsymbol{v}_{n_{ij}} \cdot \boldsymbol{n}_{ij}\right)\boldsymbol{n}_{ij} \tag{2}$$

Where the normal vector is defined, $\boldsymbol{n}_{ij} = \boldsymbol{r}_{ij}/r_{ij}$. The relative tangential velocity is

$$\boldsymbol{v}_{t_{ij}} = \boldsymbol{v}_{ij} - \boldsymbol{v}_{n_{ij}} - \frac{1}{2}(\boldsymbol{\omega}_i + \boldsymbol{\omega}_j) \times \boldsymbol{r}_{ij} \tag{3}$$

the tangential displacement vector is $\boldsymbol{t}_{ij} = \boldsymbol{v}_{t_{ij}} \Delta t$ and the tangential displacement is defined as $\delta_{t_{ij}} = \|\boldsymbol{t}_{ij}\|_2$.

3.3. Normal force

The normal interaction force on particle i from particle j is given by,

$$\boldsymbol{F}_{n_{ij}} = \boldsymbol{n}_{ij} K_n \delta_{n_{ij}}^{\frac{3}{2}} - N_{n_{ij}} \boldsymbol{v}_{n_{ij}} + \boldsymbol{F}_{coh_{ij}} \tag{4}$$

$N_{n_{ij}}$ is the normal non-linear damping coefficient and $\boldsymbol{F}_{coh_{ij}}$ is force due to cohesion.

The stiffness in the normal direction can be found as,

$$K_n = \frac{4}{3} E_{eq} \sqrt{R_{eq}} \tag{5}$$

where the equivalent Young's modulus is given by $E_{eq} = \frac{1}{\frac{1-\nu_i^2}{E_i} + \frac{1-\nu_j^2}{E_j}} = \frac{E}{2(1-\nu^2)}$ and the equivalent radius is given by, $R_{eq} = \frac{1}{\frac{1}{R_i} + \frac{1}{R_j}} = \frac{R}{2}$.

The cohesion is described by the Johnson-Kendall-Roberts (JKR) model with the factor −1.5,where the particle-particle constant cohesion force in the normal direction is defined as

$$\boldsymbol{F}_{coh_{ij}} = -1.5\pi R_{min} W \boldsymbol{n}_{ij} \tag{6}$$

$R_{min} = R$ is the minimum radius of contact, W is the cohesion parameter.

The damping coefficient in the normal direction is defined as, $N_{n_{ij}} = \frac{4}{3}\sqrt{5K_n M_{eq}}\delta_{n_{ij}}{}^{1/4} N_{n,damp}$ where $N_{n,damp} = \frac{-\ln(e_n)}{\sqrt{\pi^2 + \ln(e_n)^2}}$ and the coefficient of restitution is formally defined as $e_n = -\frac{\boldsymbol{v}_{in}}{\boldsymbol{v}_{out}}$, where v_{in} is the velocity before impact and v_{out} is the velocity after impact and the equivalent mass is given by, $M_{eq} = \frac{1}{\frac{1}{M_i} + \frac{1}{M_j}} = \frac{M}{2}$.

Note for the particle-wall interaction the radius of the wall is $R = \infty$ and the cohesion ($\boldsymbol{F}_{coh_{ij}}$) is neglected in Eq. (4).

3.4. Tangential force

The tangential force on particle i from particle j can be found as,

$$\boldsymbol{F}_{t_{ij}} = K_t \frac{\boldsymbol{t}_{ij}}{\|\boldsymbol{t}_{ij}\|_2} \delta_{t_{ij}}{}^{3/2} - N_{t_{ij}} \boldsymbol{v}_{t_{ij}} + \boldsymbol{T}_{\mathrm{rol}_{ij}} \tag{8}$$

The tangential stiffness is defined as $K_t = 8G_{eq}\sqrt{R_{eq}\delta_{n_{ij}}}$ and the equivalent shear modulus as $G_{eq} = \frac{1}{\frac{2(2-\nu_i)(1+\nu_i)}{E_i} + \frac{2(2-\nu_j)(1+\nu_j)}{E_j}} = \frac{E}{4(2-\nu)(1+\nu)}$. The $N_{t_{ij}}$ is the non-linear damping coefficient in the tangential direction and is defined as,

$$N_{t_{ij}} = \frac{4}{3}\sqrt{5K_t M_{eq}} N_{t,damp} \tag{9}$$

$N_{t,damp} = \frac{-\ln(e_t)}{\sqrt{\pi^2 + \ln(e_t)^2}}$ and the coefficient of restitution is formally defined as $e_t = -\frac{\boldsymbol{\omega}_{in}}{\boldsymbol{\omega}_{out}}$, where $\boldsymbol{\omega}_{in}$ is the angular velocity before impact and $\boldsymbol{\omega}_{out}$ is the velocity after impact.

Note that there is a maximal tangential force due to Coulomb's law,

$$\left\|\boldsymbol{F}_{t_{ij}}\right\|_2 < \left\|\mu_s \boldsymbol{F}_{n_{ij}}\right\|_2 \tag{10}$$

where μ_s is the static friction coefficient and the particle-particle static friction coefficient is denoted $\mu_{s,p-p}$ and particle-wall static friction coefficient is denoted $\mu_{s,p-w}$.

The rolling resistance for the particle-particle interaction uses is the constant torque method, defined as,

$$\boldsymbol{T}_{\mathbf{rol}_{ij}} = -\frac{\boldsymbol{\omega}_{ij}}{|\boldsymbol{\omega}_{ij}|}\mu_r R_{eq}\left|\boldsymbol{F}_{n_{ij}}\right| \tag{11}$$

The relative angular velocity between the two particles is defined as $\boldsymbol{\omega}_{ij} = \boldsymbol{\omega}_i - \boldsymbol{\omega}_j$ and the torque from the rolling resistance is $\boldsymbol{T}_{\mathrm{rol}_{ij}}$. Note for the particle-wall interaction the rolling resistance ($\boldsymbol{T}_{\mathrm{rol}_{ij}}$) is neglected in Eq. (8).

3.5. Summing the forces

Finally the total force on the i'th particle is

$$\boldsymbol{F}_i^{tot} = m_i \boldsymbol{g} + \sum_j \left(\boldsymbol{F}_{n_{ij}} + \boldsymbol{F}_{t_{ij}}\right) \tag{12}$$

where $\boldsymbol{g}$ is acceleration due to gravity. The torque on the i'th particle is

$$\boldsymbol{T}_i = -R_i \sum_j \left(\boldsymbol{n}_{ij} \times \boldsymbol{F}_{t_{ij}}\right) \tag{13}$$

From this the acceleration, velocity and position are calculated numerically by Newton second law.

3.6. Maximum time step

The maximum time step is found from the smallest value of the following three constrains; The first time constraint, τ_1 is the Rayleigh wave velocity [25,28,17]. The second constraint, τ_2 on the time step is that it takes at least 10 time-steps for the particle to move the full length of the radius. The third constrain on the time steps is τ_3, which is the duration of impact of two perfectly elastic spheres with the Hertz contact theory derived by Timoshenko [29]. Thus, the time step takes the value $\tau = \min(\tau_1, \tau_2, \tau_3)$, where in practice τ_1 is typically the limiting factor [17].

4. Result of testing the green sand and calibrating the DEM model

4.1. Standard testing of green sand (AFS)

The values from the three tests; the water content, the AFS standard 3 and 10 stroke rammer procedure can be seen in Table 1.

4.2. RST-SX: Internal friction angles (φ)

On the ring shear tester of the type RST-SX 95, five experiments were conducted and the results can be seen in Fig. 6.

The average values obtained were the internal friction angles $\mu_e = 46.5°$ (std = 2.7°), $\mu_{lin} = 28.6°$ (std = 1.6°) and $\mu_{sf} = 38.4°$ (std = 1.4°) and earlier tri-axial experimental values of $\mu_s = \tan^{-1}(29°) = 0.47$ were attained from [30]. The linearized internal friction coefficient obtained is $\mu_{lin} = \tan^{-1}(\varphi_{lin}) = 0.54$, the internal friction coefficient at steady-state flow gives a higher value, $\mu_{sf} = \tan^{-1}(\varphi_{sf}) = 0.79$, where the effective internal friction coefficient gives the highest value of $\mu_e = \tan^{-1}(\varphi_e) = 1.05$.

The cohesion value (τ_0) can be found by extrapolating the linearized yield locus (μ_{lin}) to the intersection of the yield locus with the shear stress axis. The effective angle of internal friction (φ_e) is larger compared to the angle of internal friction at steady-state flow (φ_{sf}) for the green sand and thereby the effective angle of internal friction (φ_e). The average cohesion value of the five tests was $\tau_0 = 586$ Pa with std = 51 Pa.

4.3. RST-SX: Sliding friction angles (μ)

The result from the sliding friction of the green sand on stainless steel on the ring shear tester can be seen in Fig. 7.

Using the overall average of the three tests each with six points of different normal pressure where an average angle of 19.2° with a standard deviation of 1.33° was obtained. The corresponding sliding friction coefficient of green sand on the stainless steel plate is measured $\mu_{s,p-w} = 0.35$.

4.4. Material values for simulating the experimental sand pile

Obtaining accurate DEM parameters to realistically simulate the DISAMATIC process is important but the small particle radius of 0.1 mm makes a direct numerical simulation impractical due to the large number of particles required. However the complexity of cohesion properties of their combination of water and bentonite coating coats the quartz sand and also binds the quartz sand particles together creating larger clusters of particles. This indicates that the used particle size in the calculation should be somewhat closer to the selected size of $R = 1\ mm$ in radius to represent a cluster of quartz sand particles.

The elastic properties for the steel in the chamber wall and for the sand they are selected to be of the same values as those for a similar material, brick (Fire Clay) in STAR-CCM+ cf. Table 2. It should be noticed that the choice of these values is found to be of less importance compared to the rolling resistance and cohesion value for the shape of the sand pile in [9]. This makes the sand pile experiment ideal for calibrating the values of particle-particle rolling resistance ($\mu_{r,p-p}$) and the particle-particle cohesion value (W_{p-p}) from the sand pile height (h_p).

The representative DEM particle density of green sand is found from the maximum density of the 10 strokes in the ramming station cf. Table 1, $\rho_{DEM,2D} = 2\sqrt{3}\rho_{Bulk}/\pi \approx 1720$ kg/m^3 and $\rho_{DEM,3D} = 2\sqrt{3}\rho_{Bulk}/\pi \approx 2100$ kg/m^3 assuming the maximum packing fraction (hexagonal close packing).

The coefficient of restitution (e) for both the particle-particle and particle-wall is chosen to be very small and very close to critical damping because of the high damping properties of the bentonite coated green sand.

The particle-wall static friction applied in all the simulations is $\mu_{s,p-w} = 0.35$ corresponding to the average value obtained from the ring shear tests (RST-SX) for the green sand samples interaction with a stainless steel plate. The particle-particle static friction coefficient of $\mu_{s,p-p} = 0.5$ is initially used for the calibration of the DEM simulation, and this is close to the obtained value from the ring shear test of $\mu_{lin} = 0.54$ and the value of $\mu_{lin} = 0.47$ found in [30].

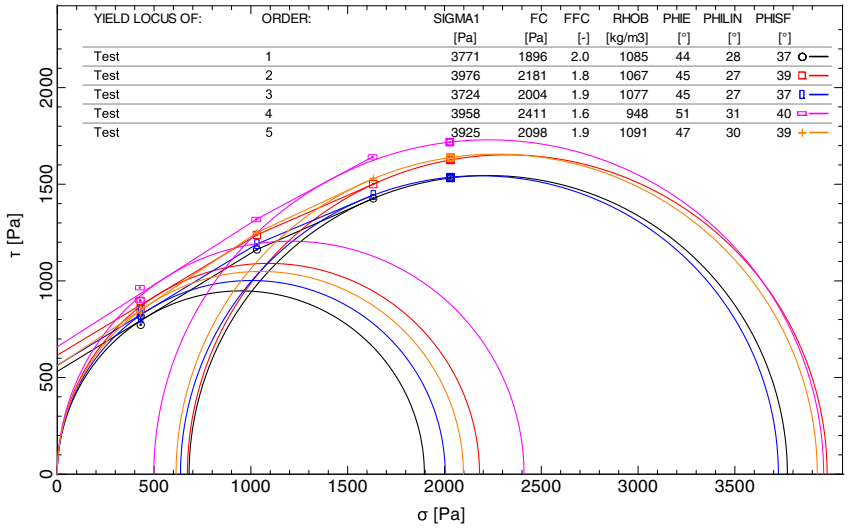

Fig. 6. Yield locus determination for green sand, five experiments was conducted on the same batch of green sand.

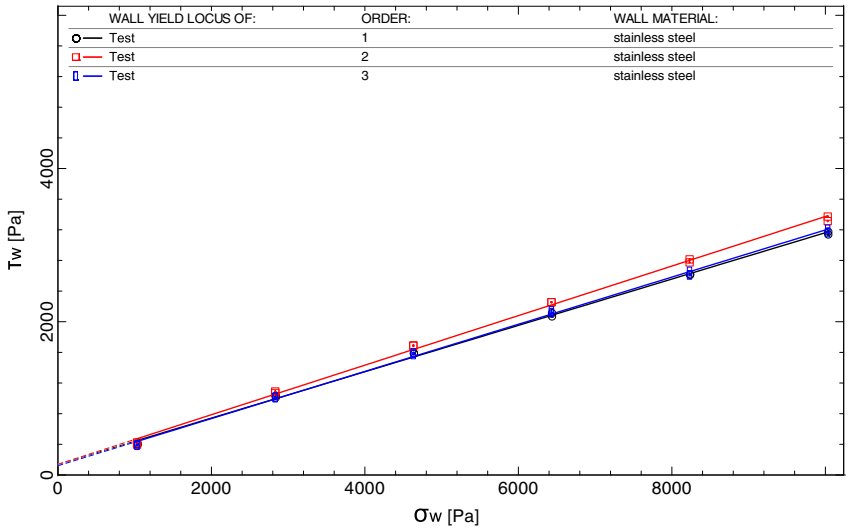

Fig. 7. The sliding friction test was conducted on the green sand interaction with a "smooth" stainless steel plate similar to the plates in the DISAMATIC chamber. Three tests were conducted on the same batch.

In the 2-D simulation the particles are injected from a line above the hopper with 100 points until the hopper is filled. To save computational time in the simulation of the 3-D hopper, the system is filled with an injector where the particles are placed randomly until the hopper is filled. For the 3-D hopper simulation a periodic boundary is applied in the z-direction (depth direction).

4.5. Result of the hopper experiment and the hopper simulation

Three sand pile experiments were conducted on the green sand batch and the average maximum height of the sand pile above the box was $h_p = 54$ mm with a standard deviation of $\sigma = 2$ mm and with an estimated tolerance precision of ± 2.0 mm. Due to the high bonding effect of bentonite, when the water content is increased, the height of the sand pile will also increase. The shape of the sand pile changes at the same time to being less conical [11].

In Fig. 8 the maximum height of the sand pile in the experiment (black line) and the DEM calibration simulations are found and compared. For the 2-D simulations a cohesion value of $W_{p\text{-}p} = 0.7$ J/m^2 results in higher sand piles than a cohesion value of $W_{p\text{-}p} = 0.5$ J/m^2 for the same rolling resistance. However, for this value the sand pile attains an unphysical shape. Based on these results the selected parameters for the 2-D simulation are: particle-particle cohesion $W_{p\text{-}p} = 0.5$ J/m^2, rolling resistance $\mu_{r,p\text{-}p} = 0.3$, static friction coefficient $\mu_{s,\ p\text{-}p} = 0.50$ (height of $h_p = 0.054$ m). The corresponding parameters for the 3-D simulation are: the particle-particle cohesion $W_{p\text{-}p} = 0.3$ J/m^2, the rolling resistance $\mu_{r,p\text{-}p} = 0.3$ and the static friction coefficient $\mu_{s,p\text{-}p} = 0.50$. Changing the particle static friction from $\mu_{s,\ p\text{-}p} = 0.50$ to $\mu_{s,\ p\text{-}p} = 0.75$ for the selected 2-D and 3-D hopper simulations changes the height of the pile less than 8%.

Fig. 9 compares the shape of the sand pile for the experiment 2-D simulation and 3-D simulation in general good agreement is observed.

Table 2
Material values for the DEM simulation of the sand pile experiments. The calibration of the 2-D simulation parameters: the rolling friction coefficient for the particle-particle interaction is varied with 4 different values, and the cohesion value for particle-particle interaction has 3 different values, giving a total of 12 simulations. For the calibration of the 3-D simulation parameters: the rolling friction coefficient for the particle-particle interaction is varied with 3 different values for one cohesion value.

Material properties	Value
Green sand particle radius (R)	0.001 m
Solid density – chamber wall (ρ_{wall})	7500 kg/m^3
Young's modulus – green sand, (E_p)	17,000 MPa
Young's modulus – chamber wall, (E_w)	200,000 MPa
Poisson ratio – green sand, (ν_p)	0.3
Poisson ratio – chamber walls,(ν_w)	0.3
Coefficient of restitution particle-particle, (e_n)	0.01
Coefficient of restitution particle-wall, (e_t)	0.01
Gravity (g)	9.82 m/s^2
Particle-Wall static friction, ($\mu_{s,p-w}$)	0.35
Particle-Particle static friction, ($\mu_{s,p-p}$)	0.50
The simulation time step, (Δt)	10^{-5} s
2-D specification	
Representative particle density – green sand ($\rho_{DEM,2D}$)	1720 kg/m^3
Particle-Particle rolling friction coefficient (μ_r)	[0.1 0.2 0.3 0.4]
Cohesion work (W_{p-p})	[0 0.5 0.7] J/m^2
3-D specification	
Representative particle density – green sand ($\rho_{DEM,3D}$)	2100 kg/m^3
Particle-Particle rolling friction coefficient (μ_r)	[0.2 0.3 0.4]
Cohesion work (W_{p-p}),	[0.3] J/m^2

4.6. Material values chosen for simulating the DISAMATIC process

The settings applied for simulating the DISAMATIC process are the rolling friction coefficient and cohesion value for particle-particle interaction which were found from calibration of the sand pile simulation. The particle-particle static friction coefficients of $\mu_{s,p\text{-}p} = 0.50$ and $\mu_{s,p\text{-}p} = 0.75$ are chosen so the simulated values are close to the interval of the obtained values from the ring shear tests of $\mu_{lin} = 0.54$ and $\mu_{sf} = 0.79$ and the lower value of $\mu_{lin} = 0.47$ found in [30]. The values from Table 2 are applied for the DISAMATIC simulations, where the final calibrated parameters for the particle-particle interactions are listed in Table 3.

5. Experimental video footage

The experimental video footage was captured with a Go-pro camera positioned in the right hand side top corner of the mould chamber and looking downwards on the flow around the ribs and cavities cf. Fig. 10.

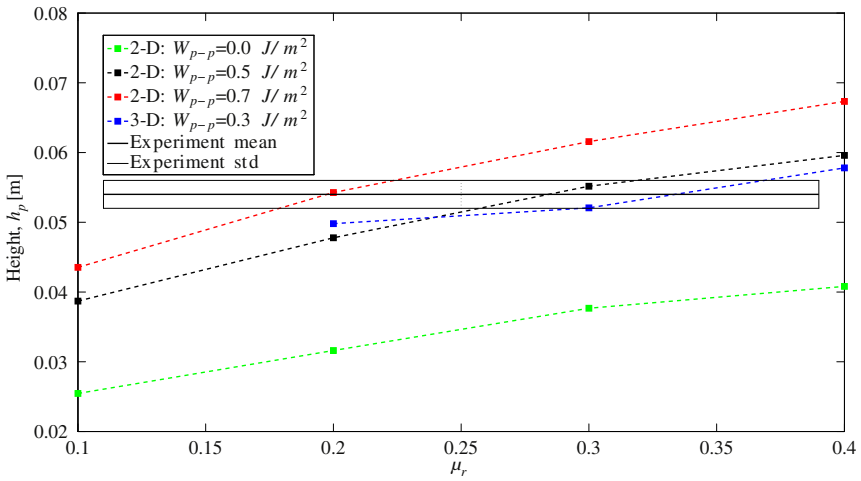

Fig. 8. The height of the simulated sand pile (h_p) as function of the particle-particle rolling resistance ($\mu_{r,\,p\text{-}p}$). The black line is the mean height of the green sand pile experiment of $h_{p,} = 0.054 \pm 0.002$ m with standard deviation of $\sigma = 0.002$ m (the two grey lines). 2-D DEM simulations have the settings of the cohesion value $W_{p\text{-}p} = 0$ J/m^2 (green dotted line), $W_{p\text{-}p} = 0.5$ J/m^2 (black dotted line) and $W_{p\text{-}p} = 0.7$ J/m^2 (red dotted line) all values simulated for the four rolling resistances of $\mu_{r,\,p\text{-}p} = 0.1$, $\mu_{r,\,p\text{-}p} = 0.2$, $\mu_{r,\,p\text{-}p} = 0.3$, $\mu_{r,\,p\text{-}p} = 0.4$ and a particle-particle static friction coefficient of $\mu_{s,\,p\text{-}p} = 0.5$. DEM simulations for the 3-D simulations have the settings of the cohesion value $W_{p\text{-}p} = 0.3$ J/m^2 (blue dotted line) for the three rolling resistances of $\mu_{r,\,p\text{-}p} = 0.2$, $\mu_{r,\,p\text{-}p} = 0.3$, $\mu_{r,\,p\text{-}p} = 0.4$ and a particle-particle static friction coefficient of $\mu_{s,\,p\text{-}p} = 0.5$. (For interpretation of the references to color in this figure legend, the reader is referred to the web version of this article.)

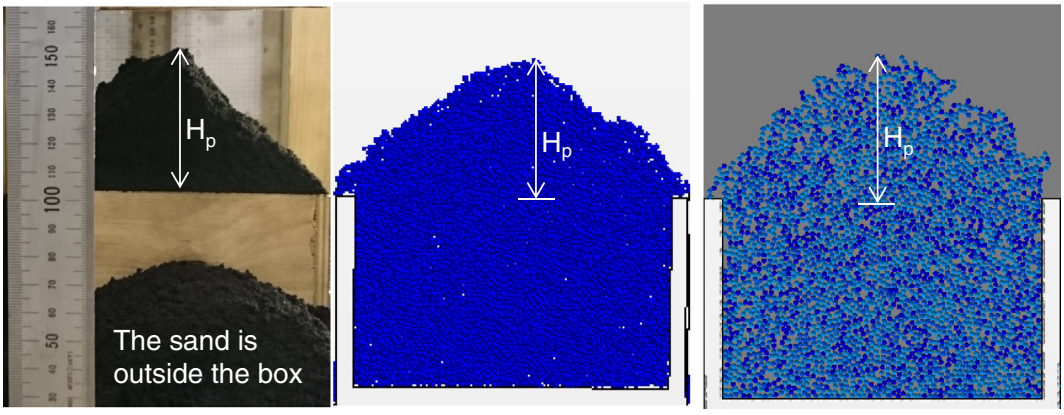

Fig. 9. (left) The sand pile experiment is compared to selected simulations, (middle) the 3-D simulation with particle-particle cohesion of $W_{p\text{-}p} = 0.3$ J/m^2, rolling resistance $\mu_{r,\,p\text{-}p} = 0.3$ and (right) the 2-D simulation particle-particle cohesion of $W_{p\text{-}p} = 0.7$ J/m^2, rolling resistance $\mu_{r,\,p\text{-}p} = 0.2$.

Table 3
The material properties of the 2-D and 3-D DEM simulations of the DISAMATIC process.

Material properties	Value
Particle-Wall static friction, ($\mu_{s,p\text{-}w}$)	0.35
Particle-Particle rolling friction coefficient ($\mu_{r,p\text{-}p}$)	0.3
Particle-Particle rolling friction coefficient ($\mu_{r,p\text{-}w}$)	Not applied
Particle-Wall cohesion work ($W_{p\text{-}w}$)	Not applied
2-D specification	
Particle-Particle static friction, ($\mu_{s,p\text{-}p}$)	0.50, 0.75
Cohesion work ($W_{p\text{-}p}$)	0.5 J/m^2
2-D Particle-Wall sensitivity analysis[a]	
Particle-Wall interaction parameters ($\mu_{r,p\text{-}w}$,$W_{p\text{-}w}$)	(0.3, 0.1 J/m^2), (0.5, 0.5 J/m^2)
3-D specification	
Particle-Particle static friction, ($\mu_{s,p\text{-}p}$)	0.50, 0.75[b]
Cohesion work ($W_{p\text{-}p}$)	0.3 J/m^2

[a] A sensitivity study of the particle-wall interaction with respect to the rolling resistance ($\mu_{r,p\text{-}w}$) and the cohesion value ($W_{p\text{-}w}$) is conducted for one of the 2-D simulations of the DISAMATIC process. The 2-D particle-wall sensitivity analysis had the particle-particle values as the other 2-D simulations with $\mu_{s,p\text{-}p} = 0.50$ and is only investigated for the compressed air pressure of 2.0 bar experiment.

[b] For the 3-D simulation with the particle-particle value static friction of $\mu_{s,p\text{-}p} = 0.75$ is only applied for simulating the 2.0 bar experiment.

The camera was run at 240 fps and the sand shot with the compressed air pressures for the successive trials were 2.0 bar, 2.5 bar and 3.0 bar.

5.1. The experimental video footage flow dynamics (t_1-t_6)

In Fig. 10, the progression of the sand shot in the chamber can be followed and the shape of the sand pile can be seen for the compressed air pressure of 2.0 bar. Eight filling times are defined and denoted t_1-t_8, where the times t_1, t_3, t_5 and t_7 denote when the sand pile reaches cavity 1, 2, 3 and 4 respectively. The times t_2, t_4 and t_6 denote when the sand pile reaches the bottom corners of ribs 1, 2 and 3 respectively and t_8 when the mould chamber is completely full. The video images at these eight times are shown for 2.0 bar in the following Fig. 10.

The times t_1-t_8 for all three experiments can be seen in Fig. 11.

In Fig. 11 it is evident that varying the air pressure affects the flow pattern. The filling times for completion of the sand shots were $t_8 = 0.74$ s for 2 bar (black curve), $t_8 = 0.65$ s for 2.5 bar (red curve) and $t_8 = 0.64$ s for 3 bar (blue curve). The filling times (t_1-t_8) and the area filled with green sand in the mould were used in the following sub-section to fit the three vertical inlet velocities and particle flow rates for the sand slot in the DEM simulations of the DISAMATIC process.

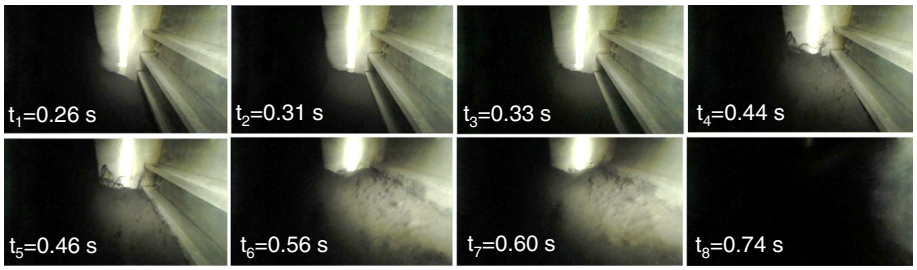

Fig. 10. The progression of the flow front starts from the upper left going to the lower right. From the experimental video footage shot with the air pressure of 2.0 bar.

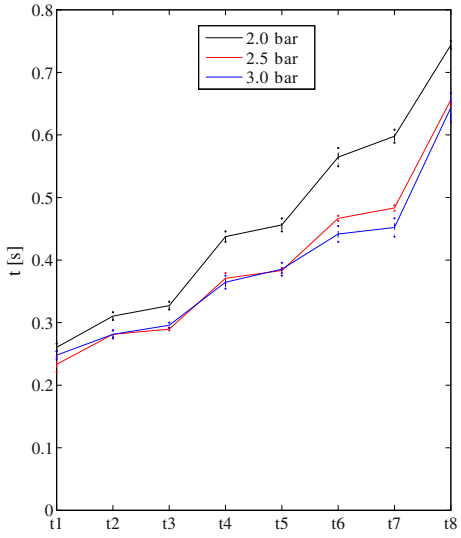

Fig. 11. The experimental progression of the sand pile flow front with respect to the eight filling times t_1-t_8 for the compressed air pressures of 2.0 bar (black curve), 2.5 bar (red curve) and 3.0 bar (blue curve). (For interpretation of the references to color in this figure legend, the reader is referred to the web version of this article.)

5.2. The geometry of the DISAMATIC process simulation

The reference geometry of the chamber is shown in Fig. 1 and Fig. 12 (left). These figures show the mould chamber with three ribs mounted on the fixed pattern plate forming four cavities positioned on the right hand side. The cross section in the middle of the chamber depth is first imported as a CAD file and subsequently selected for a 2-D section simulation and a 3-D slice simulation. The sand enters the chamber at the intersection between the hopper and chamber which is denoted the "sand slot". The dimension of the chamber is W × H × D = 0.48 m × 0.50 m × 0.60 m and the sand slot has a width of W_s = 0.04 m and a depth of 0.54 m and is centred at the middle of the chamber depth. The flow is modelled as a section (2-D) placed in the middle of the chamber depth. The 3-D slice simulation has a depth of 0.04 m placed around the middle of the chamber depth and applying a periodic boundary in the z-direction (depth direction).

5.3. Calculating the sand slot velocity and the particle flow rate

The sand slot inlet velocity, $v_y(t)$ in the DEM simulations is fitted from the experimental video footage cf. e.g., Fig. 10 with respect to the filling times t_2, t_4, t_6, t_8. The four inlet velocities (v_1, v_2, v_3, v_4) are calculated from the four filled areas (A_1, A_2, A_3, A_4) divided by the filling times of the four areas (t_2, t_4-t_2, t_6-t_4, t_8-t_6) and the sand slot width (W_s). The velocities (v_1, v_2, v_3, v_4) are assumed to vary linearly in time with a constant final velocity of v_4, cf. Fig. 12 (right).

The particle flow rate (particle/s) is obtained from the sand slot velocity from the area of the sand slot, the ideal particle packing fraction (hexagonal packing fraction), and radius of the particle.

5.4. Particle velocity distribution

The initial particle velocity in the vertical direction is given by the sand slot inlet velocity ($v_y(t)$) adding a normally distributed random

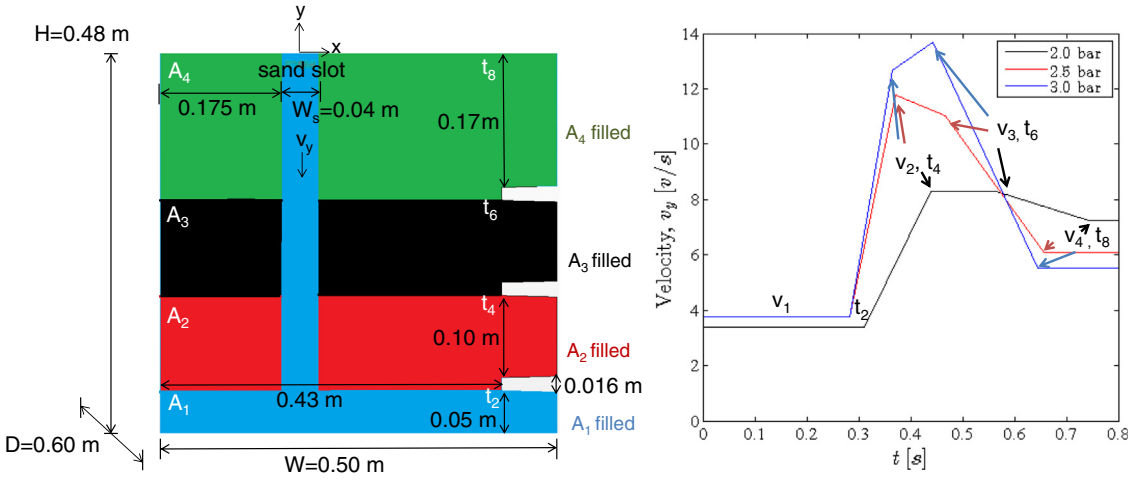

Fig. 12. (Left) From the green sand filling time of the four areas A_1-A_4 (A_1 blue, A_2 red, A_3 black, A_4 green), four velocities (v_1-v_4) can be calculated with the four selected time intervals [$0 \le t \ge t_2$, $t_2 \le t \ge t_4$, $t_4 \le t \ge t_6$, $t_6 \le t \ge t_8$]. (Right) The four velocity intervals are illustrated for the velocities (v_1, v_2, v_3, v_4) and are assumed to vary linearly in time with a constant final velocity of v_4. (For interpretation of the references to color in this figure legend, the reader is referred to the web version of this article.)

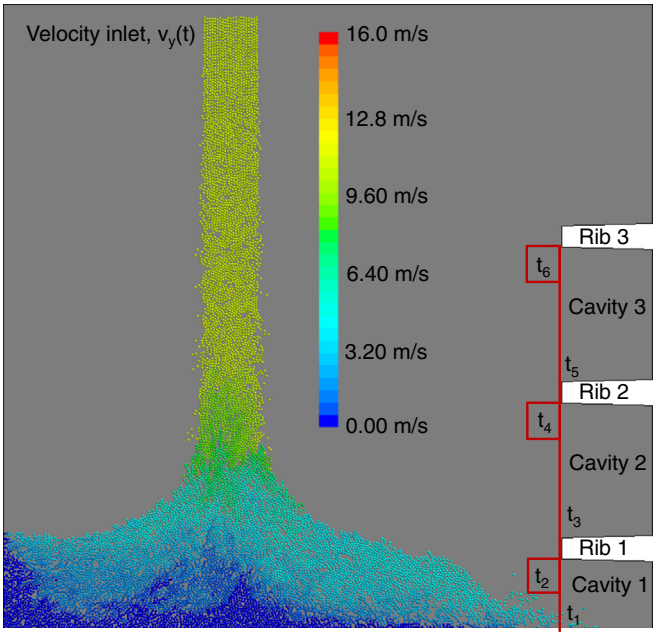

Fig. 13. Definition of the six filling times (t_1-t_6): The times t_1, t_3 and t_5 in the simulations are defined as when one particle enter cavity 1, cavity 2 and cavity 3 respectively. The times t_2, t_4 and t_6 in the simulations are defined as when one particle enters the small boxes (red boxes with area of 100 mm^2) at the rib edge of cavity 1, cavity 2 and cavity 3 respectively. The magnitude of the velocity has been plotted with a scaling of 0–16 m/s with the scale going from minimum dark blue, 0 m/s to the maximum velocity red 16 m/s. (For interpretation of the references to color in this figure legend, the reader is referred to the web version of this article.)

fluctuation with zero mean and standard deviation 0.1 m/s truncated at ± 0.2 m/s. A similar perturbation is added to the horizontal velocity ($v_x(t)$) with a mean of 0.0 m/s and with a maximum fluctuation of ± 1.0 m/s. The fluctuations emulate the random nature of the green sand flow in the chamber.

5.5. Definition of the filling times (t_1-t_6) for the DEM simulation of the DISMATIC process

The filling times t_1-t_8 are measured in the experiment, but only t_1-t_6 are defined for the simulations as seen in Fig. 13.

In Fig. 13, the time intervals are defined as when a particle crosses the red lines and goes into the boxes (t_2, t_4, t_6) and cavities (t_1, t_3, t_5).

6. Results of the simulation and the experiment for the DISAMATIC process

6.1. Comparison of the selected times (t_1-t_6) for the simulation versus the experiments

The simulations are compared to the video footage with respect to the six time intervals (t_1-t_6) in Fig. 14. The simulated filling times of (t_1-t_6) are in general in good agreement with the experimental values with small differences for the filling of t_1 and t_4-t_5 as shown in Fig. 14. The 2-D simulation with increased particle-particle static friction coefficient of $\mu_{s,\ p\text{-}p} = 0.75$ (not shown) predicts filling times with deviation less than 10% of the reference simulation ($\mu_{s,\ p\text{-}p} = 0.50$). Similar small deviations are observed in 3-D when increasing the particle-particle static friction coefficient from $\mu_{s,\ p\text{-}p} = 0.50$ to $\mu_{s,\ p\text{-}p} = 0.75$.

In addition the particle-wall sensitivity analysis simulated in 2-D for the compressed air pressure of 2.0 bar predicts filling times with deviation less than 5.0% of the reference simulation.

6.2. The sand flow profile and dynamics of the flow

In Figs. 15–17 to Fig. 17, the experiments (left) and simulations (to the right) are presented for the three selected times t_2, t_4 and t_6 and the contour of the flow profile of the sand can also be seen on the rear wall of the experiments.

In general for Figs. 15–17 the simulations show similar behaviour and filling times (t_2, t_4) as the corresponding video footage rear wall profile for the three compressed air pressures. The filling time of t_4 is consistently longer for the simulations than the experiment. Generally the sand is observed to moves more dynamically in the vertical direction for both the 2-D and 3-D simulations than in the experiments which results in stronger curvature of the flow front. The 3-D simulations predict longer filling times than the corresponding 2-D simulations.

In Fig. 18 the dynamics of the filling in the top of the chamber is investigated for the different air pressures. A slower deposition of the green sand in the larger top cavity can be seen in Fig. 18 for the 3-D simulations compared to the 2-D simulations. For 3.0 bar (Fig. 18 to the right) the 2-D has more energy than the corresponding 3-D, especially for later times where the green sand interferes with the particle jet coming from the sand slot. In general a larger scatter of particles is observed in the 3-D simulations than in the 2-D simulation, due to the extra degrees of freedom [8]. Compared to the 2.0 bar simulation a more chaotic flow front is observed for the simulated air pressures of 2.5 bar and 3 bar where the sloshing upwards at the two sides is more pronounced cf. Fig. 18.

For 2-D simulations the particle-particle static friction coefficient of $\mu_{s,\ p\text{-}p} = 0.75$ had virtually the same qualitative behaviour

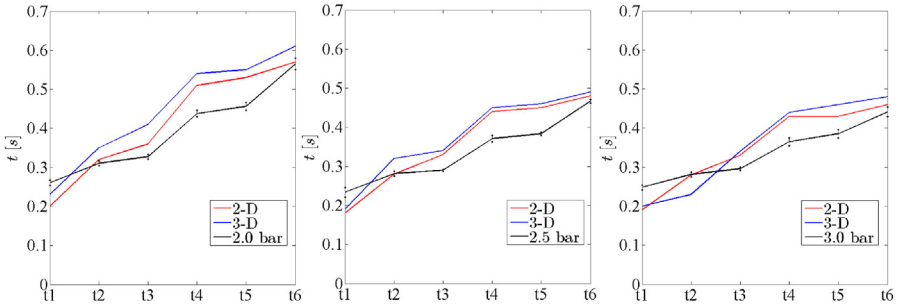

Fig. 14. Filling times obtained for 2.0 bar, 2.5 bar and 3.0 bar (from left to right). Experiments (black line), calibrated DEM simulations: 2-D (red line) and 3-D (blue line). (For interpretation of the references to color in this figure legend, the reader is referred to the web version of this article.)

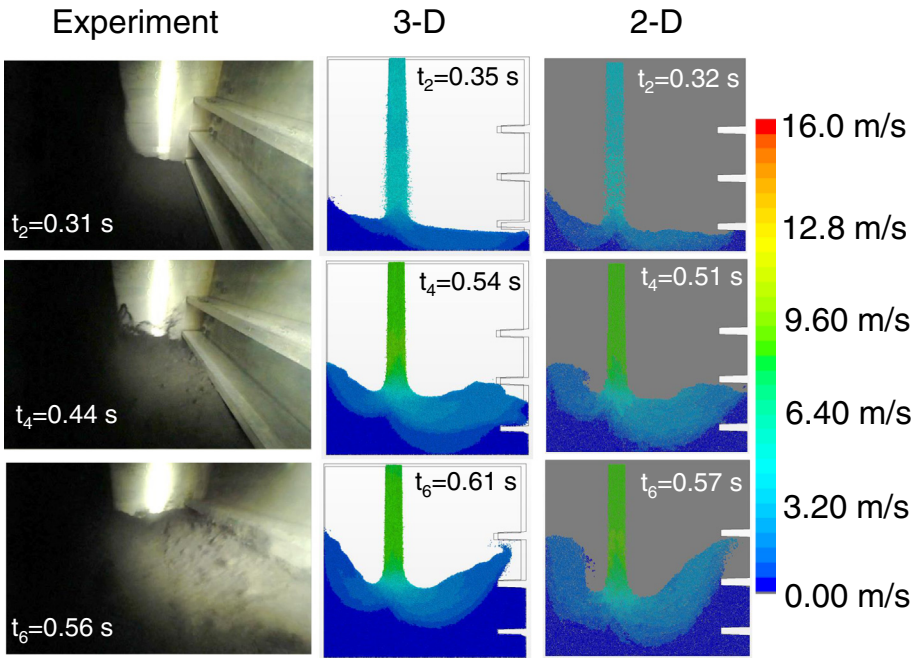

Fig. 15. Flow contours obtained for the compressed air pressure of 2.0 bar: (left) The experimental video footage, (middle) the 3-D simulation $\mu_s = 0.50$, (right) the 2-D simulation $\mu_s = 0.50$. The experiments and simulations are all presented for the three selected times t_2, t_4 and t_6 (from the upper figure to the lower figure) and the contour of the flow profile of the sand can also be seen on the rear wall. The magnitude of the velocity is plotted with a scaling of 0–16 m/s.

as $\mu_{s\ p\text{-}p} = 0.50$ shown in Figs. 15–18. For the particle-wall sensitivity study in the 2-D simulation of the compressed air pressure of 2.0 bar, incorporating the rolling resistance and cohesion had virtually the same qualitative behaviour as the reference simulation.

7. Conclusion

The main findings of the discrete element method for modelling green sand flow during production of DISA moulds are.

- The DEM models material properties was found from the experiment, where cohesion simulates the bonding effect of bentonite and water content in the creation of the sand pile showing an increase in height for the increased cohesion. The 2-D and 3-D simulation of the sand pile is in good agreement with the sand pile experiment.
- The behaviour of the filling time of the cavities in the mould is similar to the three experiments. The dynamic flow behaviour of the particles in the simulations is in general similar to that of the DISAMATIC process sand shot. More specifically, with

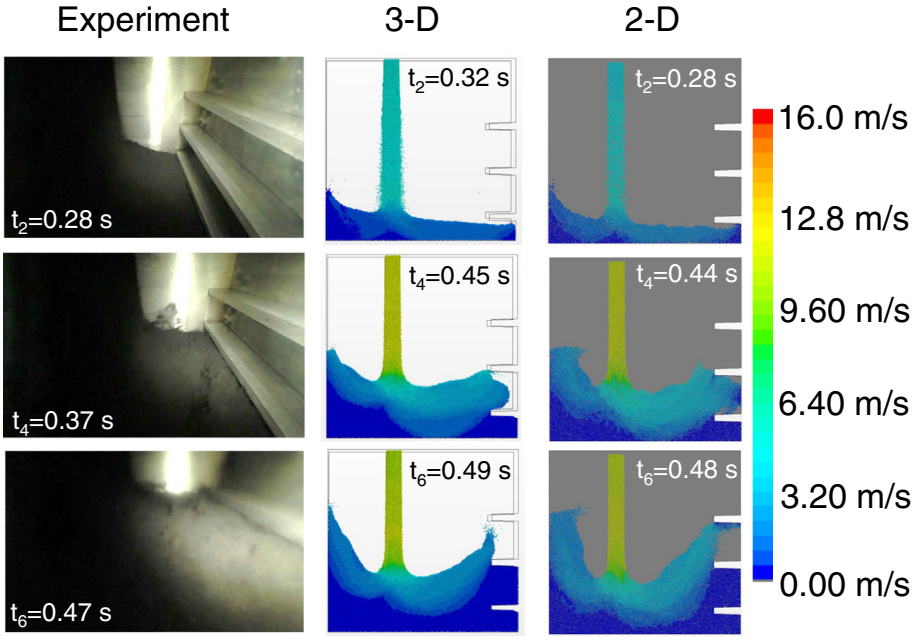

Fig. 16. Flow contours obtained for the compressed air pressure of 2.5 bar: (left) The experimental video footage, (middle) the 3-D simulation $\mu_s = 0.50$, (right) the 2-D simulation $\mu_s = 0.50$. The experiments and simulations are all presented for the three selected times t_2, t_4 and t_6 (from the upper figure to the lower figure) and the contour of the flow profile of the sand can also be seen on the rear wall. The magnitude of the velocity is plotted with a scaling of 0–16 m/s.

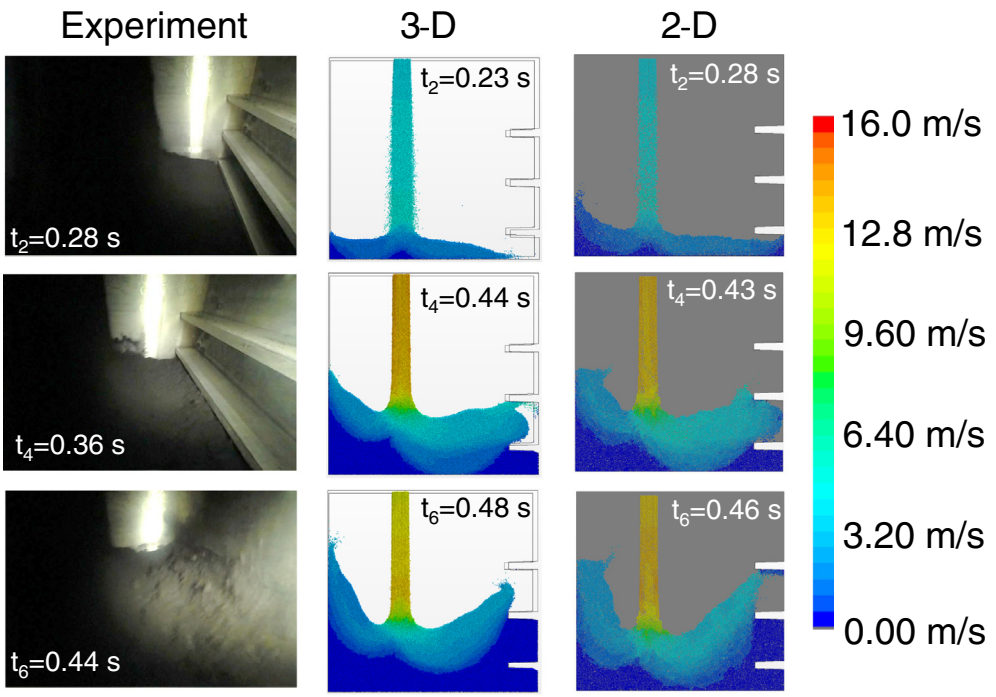

Fig. 17. Flow contours obtained for the compressed air pressure of 3.0 bar: (left) The experimental video footage, (middle) the 3-D simulation $\mu_s = 0.50$, (right) the 2-D simulation $\mu_s = 0.50$. The experiments and simulations are all presented for the three selected times t_2, t_4 and t_6 (from the upper figure to the lower figure) and the contour of the flow profile of the sand can also be seen on the rear wall. The magnitude of the velocity is plotted with a scaling of 0–16 m/s.

well selected coefficient of restitution, flow rate, damping coefficient, rolling resistance and static friction coefficient it is possible to simulate the experimental video footage very well. When the model is calibrated the flow rate and the velocity are obviously important factors for the flow dynamics during the filling of the chamber.

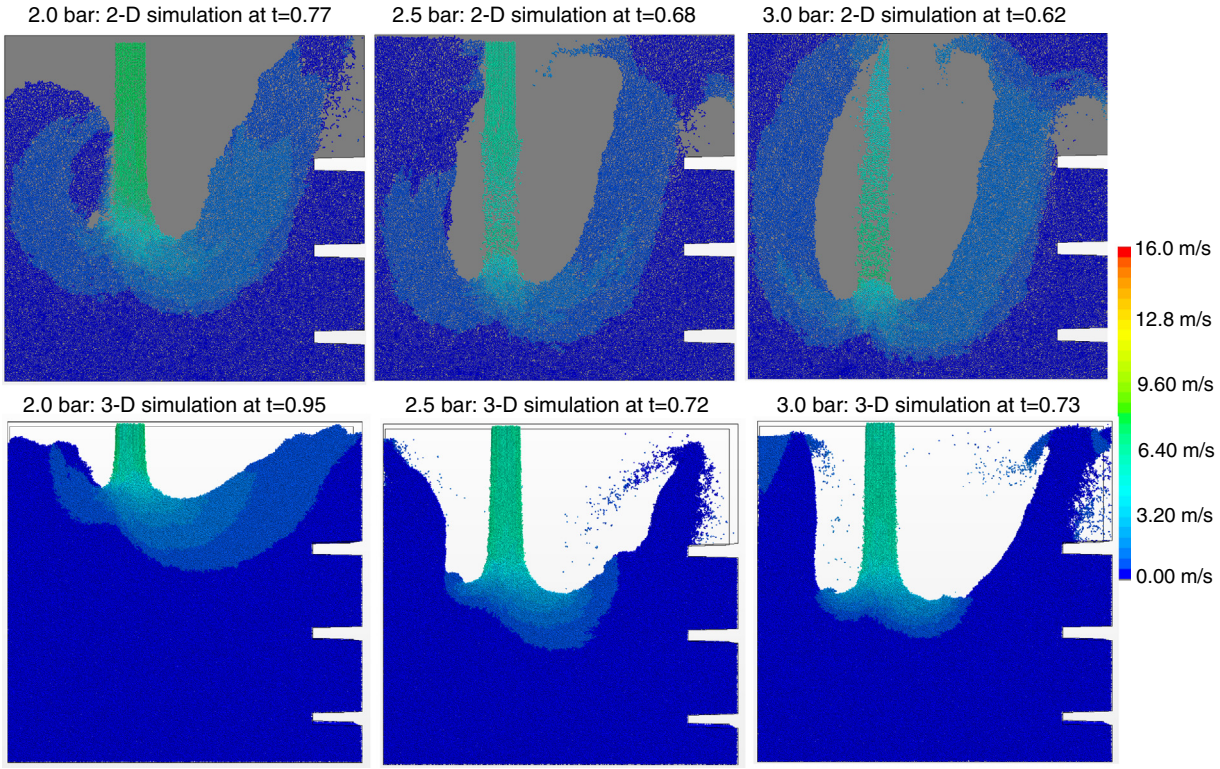

Fig. 18. The simulation for the three compressed air pressures 2.0 bar, 2.5 bar and 3.0 bar from the left to the right at (left), (middle), (right) the 2-D simulation is placed in the top and the 3-D simulation is placed in the bottom. In the top for the 2-D simulation when the sand reaches the top at $t = 0.77$ for (left), at $t = 0.68$ for (middle) and at $t = 0.62$ for (right). In the bottom for the 3-D simulation when the sand reaches the top at $t = 0.95$ for (left), at $t = 0.72$ for (middle) and at $t = 0.73$ for (right). The magnitude of the velocity is plotted with a scaling of 0–16 m/s the scale going from minimum dark blue, 0 m/s to the maximum velocity red 16 m/s.

- The increased scattering in the simulations also might be due to a smaller selected cohesion value of the 3-D simulations compared to the 2-D simulations. Although differences are seen from 2-D to the 3-D simulation the results remains in good agreement and the fast execution of 2-D simulations can still be used for parameter studies in simple geometries.
- A sensitivity study of the particle-wall interaction parameters: the rolling resistance and cohesion was performed and it was found that the quantitative and qualitative behaviour are virtually the same as the reference 2-D DISAMATIC simulation. Thereby these particle-wall parameters are of lesser importance for simulating the DISAMATIC process.
- It is found that the geometrical configuration as well as the applied compressed air pressure is highly affecting the filling pattern of the mould. More specifically, the lower compressed air pressure of 2.0 bar gives a slower deposition of green sand in general and in the top cavities in particular. The compressed air pressure and thereby the green sand velocity is of great importance especially for the filling of the top part of the mould.

Funding

The study was supported by Innovation Fund Denmark project [Grant number. 1355-00087B] in collaboration with the Danish company "DISA Industries A/S" in the period 15-08-2013 to 15-08-2016.

Acknowledgement

A thanks to Lars Georg Kiørboe for the use of the Ring shear tester at DTU CHEMICAL ENGEERING, Department of Chemical and Biochemical Engineering.

A thanks to Niels Tiedje at DTU MECHANICAL ENGINEERING Department of Mechanical Engineering for the use of the foundry equipment.

References

[1] H.P. Zhu, Z.Y. Zhou, R.Y. Yang, A.B. Yu, Discrete particle simulation of particulate systems: a review of major applications and findings, Chem. Eng. Sci. 63 (2008) 5728–5770, http://dx.doi.org/10.1016/j.ces.2008.08.006.
[2] H.P. Zhu, Z.Y. Zhou, R.Y. Yang, A.B. Yu, Discrete particle simulation of particulate systems: theoretical developments, Chem. Eng. Sci. 62 (2007) 3378–3396, http://dx.doi.org/10.1016/j.ces.2006.12.089.
[3] A. Di Renzo, F.P. Di Maio, Comparison of contact-force models for the simulation of collisions in DEM-based granular flow codes, Chem. Eng. Sci. 59 (2004) 525–541, http://dx.doi.org/10.1016/j.ces.2003.09.037.
[4] P.W. Cleary, Industrial particle flow modelling using discrete element method, Eng. Comput. 26 (2009) 698–743, http://dx.doi.org/10.1108/02644400910975487.
[5] J.H. Walther, I.F. Sbalzarini, Large-scale parallel discrete element simulations of granular flow, Eng. Comput. 26 (2009) 688–697, http://dx.doi.org/10.1108/02644400910975478.
[6] J.P. Longmore, P. Marais, M.M. Kuttel, Towards realistic and interactive sand simulation: a GPU-based framework, Powder Technol. 235 (2013) 983–1000, http://dx.doi.org/10.1016/j.powtec.2012.10.056.
[7] N. Govender, D.N. Wilke, S. Kok, Blaze-DEMGPU: Modular High Performance DEM Framework for the GPU Architecture, SoftwareX, 2016 http://dx.doi.org/10.1016/j.softx.2016.04.004.
[8] N. Govender, R.K. Rajamani, S. Kok, D.N. Wilke, Discrete element simulation of mill charge in 3D using the BLAZE-DEM GPU framework, Miner. Eng. 79 (2015) 152–168, http://dx.doi.org/10.1016/j.mineng.2015.05.010.
[9] J. Rojek, F. Zarate, C.A. de Saracibar, C. Gilbourne, P. Verdot, Discrete element modelling and simulation of sand mould manufacture for the lost foam process, Int. J. Numer. Methods Eng. 62 (2005) 1421–1441, http://dx.doi.org/10.1002/nme.1221.
[10] C.J. Coetzee, D.N.J. Els, Calibration of discrete element parameters and the modelling of silo discharge and bucket filling, Comput. Electron. Agric. 65 (2009) 198–212, http://dx.doi.org/10.1016/j.compag.2008.10.002.
[11] H. Makino, Y. Maeda, H. Nomura, Computer simulation of various methods for green sand filling, Trans. Am. Foundry Soc. 110 (2002) 1–9.
[12] Y. Maeda, Y. Maruoka, H. Makino, H. Nomura, Squeeze molding simulation using the distinct element method considering green sand properties, J. Mater. Process. Technol. 135 (2003) 172–178, http://dx.doi.org/10.1016/S0924-0136(02)00872-5.
[13] E. Hovad, Flow dynamics of green sand in the DISAMATIC moulding process using discrete element method (DEM), IOP Conf. Ser. Mater. Sci. Eng. 84 (2015).
[14] A.F. Society, Mold & Core Test Handbook, 4th Edition American Foundry Society, 2015.
[15] D. Schulze, J. Schwedes, J.W. Carson, Powders and Bulk Solids: Behavior, Characterization, Storage and Flow, 2008 http://dx.doi.org/10.1007/978-3-540-73768-1.
[16] D. Schulze, Flow Properties of Powders and Bulk Solids, Braunschweig/Wolfenbu Ttel, Ger. Univ, 2006 1–21http://dietmar-schulze.de/grdle1.pdf.
[17] STAR-CCM+, USER GUIDE STAR-CCM+, Version 8.02, 2013.
[18] P.A. Cundall, O.D.L. Strack, A discrete numerical model for granular assemblies, Géotechnique. 29 (1979) 47–65, http://dx.doi.org/10.1680/geot.1979.29.1.47.
[19] H. Hertz, Über die Berührung fester elastischer Körper, J. Für Die Reine Und Angew. Math. 171 (1881) 156–171, http://dx.doi.org/10.1515/crll.1882.92.156.
[20] Y. Tsuji, T. Tanaka, T. Ishida, Lagrangian numerical simulation of plug flow of cohesionless particle in a horizontal pipe, Powder Technol. 71 (1992) 239–250.
[21] D. Zhang, W.J. Whiten, The calculation of contact forces between particles using spring and damping models, Powder Technol. 88 (1996) 59–64, http://dx.doi.org/10.1016/0032-5910(96)03104-X.
[22] G. Hu, Z. Hu, B. Jian, L. Liu, H. Wan, On the determination of the damping coefficient of non-linear spring-dashpot system to model Hertz contact for simulation by discrete element method, 2010 WASE Int, Conf. Inf. Eng. 295–298 (2010) http://dx.doi.org/10.1109/ICIE.2010.247.
[23] Y.C. Zhou, B.D. Wright, R.Y. Yang, B.H. Xu, A.B. Yu, Rolling friction in the dynamic simulation of sandpile formation, Physica A 269 (1999) 536–553, http://dx.doi.org/10.1016/S0378-4371(99)00183-1.
[24] J. Ai, J.F. Chen, J.M. Rotter, J.Y. Ooi, Assessment of rolling resistance models in discrete element simulations, Powder Technol. 206 (2011) 269–282, http://dx.doi.org/10.1016/j.powtec.2010.09.030.
[25] K.L. Johnson, Contact Mechanics, 1985 http://dx.doi.org/10.1115/1.3261297.
[26] L.E. Silbert, D. Ertaş, G.S. Grest, T.C. Halsey, D. Levine, S.J. Plimpton, Granular flow down an inclined plane: Bagnold scaling and rheology, Phys. Rev. E Stat. Nonlinear Soft Matter Phys. 64 (2001) 051302, http://dx.doi.org/10.1103/PhysRevE.64.051302.
[28] L. Rayleigh, On Waves Propagated along the Plane Surface of an Elastic Solid, Proc. Lond. Math. Soc. s1–17 (1885) 4–11, http://dx.doi.org/10.1112/plms/s1-17.1.4.
[29] S. Timoshenko, J.N. Goodier, Theory of Elasticity, 1986 http://dx.doi.org/10.1007/BF00046464.
[30] J. Frost, M.J. Hillier, I. Holubec, The mechanics of green molding sand, AFS Trans. 75 (1967) 126–132.

E. Hovad, born in Fredericia, Denmark 1982, obtained his M.Sc. in Mathematical Modelling and Computing (MMC) from the Technical University of Denmark (DTU) in 2011with selected courses related to scientific computing and fluid dynamics. He is currently working as an industrial PhD student simulating flow dynamics of green sand in the DISAMATIC moulding process, for the Danish company DISA Industries A/S and the Department of Mechanical Engineering at DTU.

J. Spangenberg, born in Denmark 1982, obtained his M.Sc. in civil engineering in 2009 and his Ph.D. in mechanical engineering in 2012 both from the Technical University of Denmark (DTU). Subsequently, he was a postdoctoral research associate at the civil and environmental engineering department at Princeton University until 2014 where he was appointed assistant professor at the mechanical engineering department at DTU. His research interests are computational fluid dynamics, complex fluids, granular materials and process optimization.

P. Larsen, Born in Denmark, 1971, obtained his M.Sc. in process technology in 1996 and his industrial PhD in 2004 from Technical University of Denmark (DTU) in collaboration with DISA Industries A/S. He has been working for DISA Industries A/S for the last 19 years in various positions. His has also been a supervisor for several Ph.d. projects, e.g. "New Sol-Gel coatings to improve casting quality".

J.H. Walther is professor of fluid mechanics at the Department of Mechanical Engineering at the Technical University of Denmark, and research associate at the Computational Science and Engineering Laboratory at ETH Zurich, Switzerland. His research areas include the development of high order Lagrangian methods in computational fluid dynamics, efficient implementation of these methods on modern computer architectures, and the generation and analysis of data through simulations for problems in fluid mechanics. Walther holds a PhD degree in mechanical engineering from the Technical University of Denmark.

J. Thorborg, born in Denmark 1972, studied at the Technical University of Denmark, where he obtained his M.Sc. in 1997 and his Ph.D. in 2001 in mechanical engineering. During his Ph.D. project and subsequent postdoctoral fellowship he worked in the field of solid mechanics and constitutive modelling of high temperature processes. He joined the development group at MAGMA GmbH in 2004 and today he is working as a research and developer on the MAGMA stress module.

J.H. Hattel, born in Copenhagen, Denmark 1965, obtained his M.Sc. in structural engineering in 1989 and his Ph.D. in mechanical engineering in 1993 both from the Technical University of Denmark (DTU). He currently holds a full professorship in modelling of manufacturing processes at the Department of Mechanical Engineering, DTU. His research interests are modelling of processes like casting, joining, composites manufacturing and additive manufacturing. This involves the use of computational methods within the disciplines of heat transfer, fluid dynamics, solid mechanics as well as materials science. Applications range from microelectronics over automotive industry to large structures like wind turbines.